EXPERIMENTAL STUDY ON HEAT TRANSFER AND FLUID FLOW ENHANCEMENT OF A SPHERICAL SHAPE OBSTACLE SOLAR AIR PASSAGE

Ashok Kumar BHARDWAJ[1], Anil KUMAR[1], Rajesh MAITHANI[2], Raj KUMAR[1], Sunil KUMAR[1], Ranchan CHAUHAN[1]*

[1]School of Mechanical and Civil Engineering, Shoolini University, Solan, India

[2]Department of Mechanical Engineering, DIT, University, Deharadun, India

[*]Corresponding author; E-mail: anilkumar88242@gmail.com

This paper presents the outcome of experimental examined of Nusselt number and friction factors in a spherical obstacles solar air passage. Investigation has been performed to examine the thermal and hydraulic data from a solar air passage with spherical obstacles on the heated wall. The Reynolds number base on the hydraulic diameter of the solar air passage varied from 45,00 to 16,500, relative sphere diameter varied from 0.130 to 0.217, stream wise spacing of 0.152 and span wise spacing of 0.173. Experimental results pertinent to heat transfer and pressure drop was determined for various sets of roughness and flow parameters. The experimental results show that the heat transfer is increased around 4.7 times than plane surface solar air passage. The thermal and hydrodynamic performance parameter based on equal pumping power was found to be highest for spherical shape dia of 0.195. The superior value of overall thermal performance parameter is 2.83 corresponding to spherical shape dia of 0.195.

Key words*: Thermal behaviour, flow passage, sphere diameter, stream wise spacing*

Introduction

Renewable energy can minimize our dependency on fossil fuels, thereby, renewable energy are getting importance in the recent years because energy can renewed and will never run out. Renewable energy is ecofriendly and results in little to no effect to the environment [1]. Out of many renewable energies, solar energy is considersable to be clean source of energy and available on every part of the world [2]. Solar energy is exploited in many application, included heating purposes and generation of electricity. Solar air heater is the cheapest and extensively used solar energy collection device for drying of agricultural products, space heating, seasoning of timber and curing of industrial products. The use of an artificial roughness on a surface is an effective technique to enhance the rate of heat transfer to fluid flow in the duct of a solar air heater [3]. Use of rib roughness in solar air heater has been topic in research for the last thirty years. The roughness, on the absorber plate can be provided by several methods such as sand blasting, machining, casting, forming, welding ribs and or fixing thin circular wires. The use of artificial roughness in different forms and shapes is the most effective and economic way of improving the performance of a solar air heater [4]. A lot of experimental investigations involving roughness elements of different shapes, sizes and orientations with respect to flow direction have been carried out in order to obtain an optimum arrangement of roughness element geometry. The techniques of local heat transfer improvement attract the interests of researchers. Ribs are often used to improve local heat transfer among the wall and fluid because they cause stream separation and reattachment, consequently resulting in destroying the laminar viscous layer [5].

Park et al. [6] experimentally investigated the heat transfer and pressure drop in a duct with three serial perforated blockages equipped with staggered jets. Eight types of jet holes and three types of side walls, including dimpled walls, were tested. For heat transfer measurements, the transient liquid crystal technique was used. Reynolds numbers based on the hydraulic diameter of the duct and inlet velocity ranged from about 10,000-30,000. Experimental results showed that the Nusselt number ratios decreased as the Reynolds number increased, and the friction factor ratios increased as the Reynolds number increased.

Sangtarash et al.[7] numerical and experimental models have been developed to investigate the effect of adding an in-line and staggered arrangement of dimples and perforated dimples to multi-louvered fins on the heat transfer augmentation and the pressure drop of the air flow through a multi-louvered fin bank. Three-dimensional simulations of single row of louvers were conducted for the given geometries. Simulations were performed for different Reynolds numbers. The simulations revealed that the heat transfer and temperature augmentations occur due to the existence of a circulation region that is created by the dimple. The results demonstrate that adding dimples on the louver surface increases the j factor and the f factor. Likewise, adding perforation to the dimples results in the same increase.

Bhushan and Singh [8] experimentally investigated the performance of a staggered dimple type roughness solar air passage. The outcome indicates that the greatest improvement of Nu_{rs} and f_{rs} factor was 3.12 and 4.16 times respectively in comparison to smooth passage. Chang et al. [9] examine the comparative full-field Nu_{rs} distribution on two opposing improved passage walls, including f_{rs} and the thermal performance factor of the two radially rotating obstacles passage with and without dimpled obstacles. Shen et al. [10] examine the effect of rotation on fluid stream and heat transfer performance of turbine blade with U-shaped passage with the combined structure of obstacles, dimples or protrusions. The outcome shows that rib-protrusion structure found to be the most efficient structure while rib-dimple structure has only minor advantage than ribbed passage. Kumar and Kim [11] investigated the thermal hydraulic performance of a three dimensional obstacles-roughened solar air passage having W_P/H_P of 12.0. They found that thermal hydraulic performance for V-pattern shaped obstacles combined with dimpled obstacles is superior as compared with dimpled obstacles shape and V-pattern obstacles shape solar air passage. Lian et al. [12] investigated Nu_{rs} and f_{rs} behaviours of air stream through a passage with hemispherical protrusion/dimple on the heated plate. The outcome shows that the hemispherical dimple roughened air passage is the better choice as compared with smooth passage.

Negi and Pattamatta [13] deal with shape determination of dimples on the target plane in multi-jet impingement $Nu_{rs.}$ They revealed that the standard deviation in Nu_{rs} was considerably higher than the reference spherical dimpled profile and the optimized dimple profile shows highest local Nu_{rs} values calculated to the reference semi-circular dimpled plate optimized form which can be used to get better local temperature hot spots on target surface. Jin et al. [14] presented a numerical study of Nu_{rs} and f_{rs} characteristics in a SAP channel having multi V-shaped ribs on the absorber plate. It was found that for the range of investigated factors the highest value of the η_P parameter was achieved to be 1.93. Ekadewi et al. [15] numerically investigated the influence of delta-shaped obstacles spacing on Nu_{rs} and pressure drop in v-corrugated canal of SAP. Authors obtained that Nu_{rs} was improved by 3.46 times and f_{rs} was increased upto19.9 times.

The literature survey shows that obstacles of dimple, hemispherical, V-type, protrusion and multipe type shapes have been investigated previously which are common shape. In order to increase heat transfer further sperical obstacles have been investigated in this work with aim of different sphere diameter would contribute the turbulence in the flow resulting high heat transfer rate from heated plate. In this regards, experimental study has been conducted to investigate the effect of relative sphere diameter of obsctales attached to heated plate on thermal behaviour.

Range of parameter

The geometrical parameters for the solar air passage with spherical obstacles are hydraulic diameter of passage (D_H) of 46.15, height of passage (H_P) of 25mm, width of passage (W_P) of 300 mm and length of passage (L_P) of 2395 mm. The dimnesionless parameters are relative sphere diameter (D_S/D_H), stream wise spacing (X_S/D_s) and span wise spacing (Y_S/D_s). In this experimental investigation the solar air passage has L_t = 1100 mm, H_P is adjusted = 50mm and W_P is set = 300mm and the D_H = 46.15mm and different diameter of sphere (D_S). The ranges of different parameters are depicted in Table.1. The shematic and photographic view of spherical shape obtacles are presented in Fig.1 (A-B).

Table.1 Ranges of spherical obstales parameters.

Sr.No.	Parameter	Range
1.	D_S/D_H	0.130-0.217
2.	X_S/D_s	0.152
3.	Y_S/D_s	0.173
4.	Re	4,500-16,500

Experimental program and procedure

Experimental approach has been adopted to produce the data in form of Nu_{rs} and f_{rs} for air passage with spherical shape obstacle roughness to search the effect of D_S/D_H and Re on Nu_{rs} and f_{rs}. The experimental study encompasses the fabrication and installation of indoor test facility. The experimental setup has been validated by comparing experimental data collected on without speherical obstacle wall with the available standard data. After validation of experimental setup, extensive experimentations have been conducted on spherical shape obstacle to produce raw data on heated wall temperatures, air stream rates, and entrance and exit temperature of air and pressure drop across the passage under stable conditions. To examine the influence of spherical shape obstacle turbulent promoter on Nu_{rs} and f_{rs} of air stream, an experimental setup was designed and made-up according to ASHRAE standard [16]. A schematic diagram of an experimental set up is shown in Fig.2. The experimental setup comprised a rectangular wooden channel coupled to a centrifugal blower through a circular galvanized iron (GI) pipe. The rectangular channel had W_P of 300 mm, H_P of 30 mm, and W_P/H_P of 10. The examination was carried out to achieve the experimental values for Nu_{rs} and f_{rs} in an air stream passage provided with spherical shape obstacle to enhance Nu_{rs} and f_{rs} descriptions with respect to individual obstacle deviations. To measure the temperature at various diverse locations of the plate and the air at entrance and exit divisions, 0.3 mm diameter cali-brated copper constantan thermocouples have been inserted, the other end of these have been connected to digital micro voltmeter (DMV) to exemplify the temperature in ^{o}C. Before installing the thermocouples in place, they were calibrated under similar environmental conditions using a temperature calibrator for an accuracy of ±0.1 ^{o}C. The pressure drop across the test division was evaluated using micromanometer having least count of 0.1 Pa.

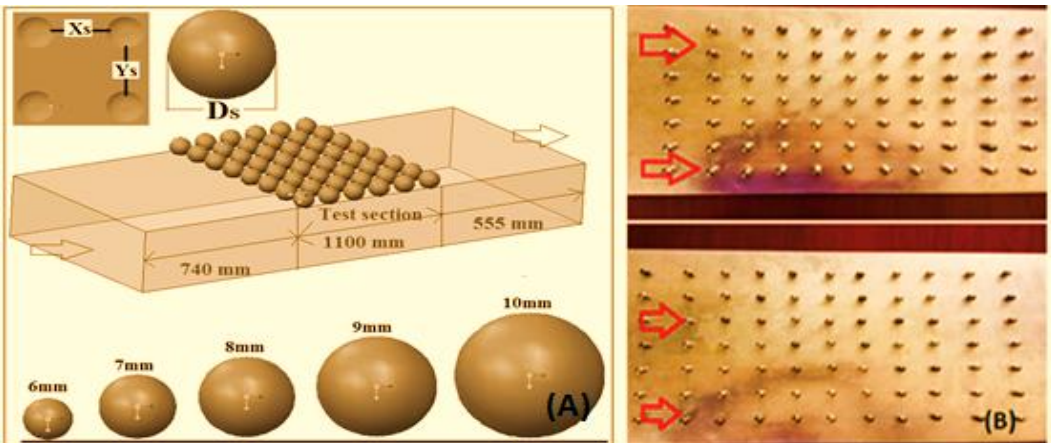

Fig.1 (A) Discussed speherical shapes parameters (B) Photograpic view of spherical roughened shape absorber plate.

The manufacturing and the appropriate setting of the experimental test setup were performed, which were validated with existing criterion data on the air passage with smooth surface passage. The optimal validation was achieved to perform advanced examinations with spherical shape obstacle. The testing for air temperature at the entry of the passage and the exit, pressure drop of air from corner to corner of the passage, and the heated wall temperature have been approximated, which is necessary to meet the aims of the investigation. In order to examine the influence of spherical shape obstacle, flat solar air rectangular passage functioning under same flow situations was also investigated. Before performing each investigational run, large care was taken to ensure appropriate functioning of all apparatus and that there was no seepage at the joints in the testing setup.

The equivalent instruments provided the data beneath stable condition which was supposed to have been attained when there was no appreciable difference in passage air and collector plate temperature was noticed over a time period of larger than 12 min. The following amount of data was reported for each:

I. Pressure head variation across the orifice plate in order to determine the air flow rate.
II. Heated plate temperatures at variant plate positions.
III. Temperatures of inlet air.
IV. Temperatures of passage air.
V. Pressure head drop across the test segment.

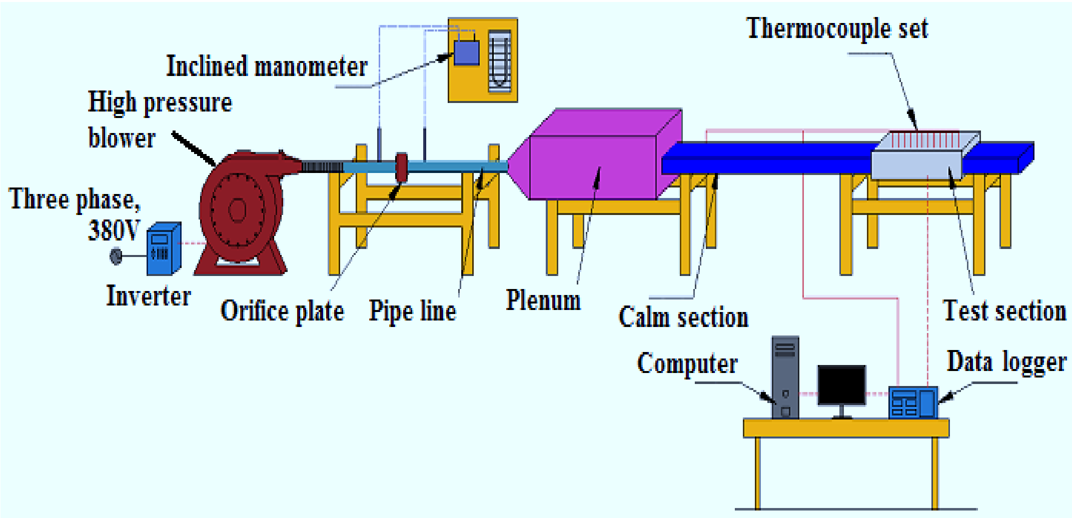

Fig.2 Scematic of experimental setup.

Data reduction

The data composed have been used to determine Nusselt number and pressure drop. Relevant expressions for the computation of the above parameters and some intermediate parameters have been given below.

The mean temperature of the plate is the average of all temperatures of the heated plate:

$$T_p = \frac{\sum T_{pi}}{N} \qquad (1)$$

The mean air temperature is a simple arithmetic mean of the inlet and outlet temperature of air flowing through the test section:

$$T_f = \frac{T_i + T_o}{2} \qquad (2)$$

where $T_o = (T_{O1} + T_{O2} + T_{O3})/3$, $T_i = T_{A1}$.

Mass flow rate of air (m_a) has been calculated from the pressure drop measurement across the calibrated orifice meter by using the following formula:

$$m_a = C_{do} A_o \left[\frac{2\rho_a (\Delta p)_0}{1 - \beta_R{}^4}\right]^{0.5} \qquad (3)$$

where $(\Delta p)_0 = 9.81.(\Delta p)_0 \rho_a m_a.Sin\theta$.

The velocity of air (V) is calculated from the mass flow rate and given by

$$V = \frac{m_a}{\rho_a W_P H_P} \qquad (4)$$

The hydraulic diameter (D_H) is given by

$$D_{hd} = \frac{4.(W_P.H_P)}{2.(W_P + H_P)} \qquad (5)$$

The Reynolds number (Re) of the air flow in the rectangular channel is determined as

$$Re = \frac{V.D_H}{\nu_a} \qquad (6)$$

The friction factor (f) is calculated from the measured value of $(\Delta_p)_d$ across the test section length using the Darcy equation as

$$f = \frac{2(\Delta_p)_d D_H}{4\rho_a L_t V^2} \qquad (7)$$

where $(\Delta_p)_d = 9.81.(\Delta_h)_d.D_H \rho_a m_{a.}$

The useful heat gained by air is calculated as

$$Q_u = m_a c_p (T_0 - T_i) \qquad (8)$$

The heat transfer coefficient for the heated test section has been calculated from

$$h_t = \frac{Q_u}{A_p.(T_p - T_f)} \qquad (9)$$

The h_t can be used to determine the (Nu), which is given by

$$Nu = \frac{h_t D_H}{K_a} \qquad (10)$$

Uncertainties analysis

Uncertainty is the possible numerical value of the error encountered during experimentation. To evaluate uncertainty involve in this experiment method suggested by Kline and McClintock [17] is used. If the data of any parameter is calculated using certain measured quantities then error in measurement of “y” (parameter) is given as follows.

$$\frac{\delta y}{y} = \left[\left(\frac{\delta y}{\delta x_1}\delta x_1\right)^2 + \left(\frac{\delta y}{\delta x_2}\delta x_2\right)^2 + \left(\frac{\delta y}{\delta x_3}\delta x_3\right)^2 + \cdots + \left(\frac{\delta y}{\delta x_n}\delta x_n\right)^2\right]^{0.5} \qquad (11)$$

Where, $\delta x_1, \delta x_2, \delta x_3$, …. δx_n are the possible error in measurement of x_1, x_2, x_3, …..x_n,

δ_y is the absolute uncertainty and $\frac{\delta_y}{y}$ is known as relative uncertainty.

The important parameters considered for the calculation of uncertainty are: Reynolds number, Heat transfer coefficient, Nusselt number, friction factor etc.

1. Uncertainty in Area of absorber plate

$A_p = W_P \times L_t$

$$\frac{\delta A_p}{A_p} = \left[\left(\frac{\delta L_t}{L_t}\right)^2 + \left(\frac{\delta W_P}{W_P}\right)^2\right]^{0.5} \qquad (12)$$

2. Uncertainty in Area of flow

$A_p = W_P \times H_P$

$$\frac{\delta A_p}{A_p} = \left[\left(\frac{\delta H_P}{H_P}\right)^2 + \left(\frac{\delta W_P}{W_P}\right)^2\right]^{0.5} \qquad (13)$$

3. Uncertainty in mass flow rate measurement

$$m_a = C_{do} A_o \left[\frac{2\rho_a (\Delta p)_0}{1 - \beta^4}\right]^{0.5}$$

$$\frac{\delta m_a}{m_a} = \left[\left(\frac{\delta C_{do}}{C_{do}}\right)^2 + \left(\frac{\delta A_o}{A_o}\right)^2 + \left(\frac{\delta \rho_a}{\rho_a}\right)^2 + \left(\frac{\delta (\Delta p)_0}{(\Delta p)_0}\right)^2\right]^{0.5} \qquad (14)$$

4. Uncertainty in measurement of air velocity in channel

$$V = \frac{m_a}{\rho_a \times W_P \times H_P}$$

$$\frac{\delta V}{V} = \left[\left(\frac{\delta m_a}{m_a}\right)^2 + \left(\frac{\delta \rho_a}{\rho_a}\right)^2 + \left(\frac{\delta W_P}{W_P}\right)^2 + \left(\frac{\delta H_P}{H_P}\right)^2\right]^{0.5} \quad (15)$$

5. Uncertainty in useful heat gain

$$Q_u = m_a c_p (T_0 - T_i) = m_a c_p \Delta T$$

$$\frac{\delta Q_u}{Q_u} = \left[\left(\frac{\delta m_a}{m_a}\right)^2 + \left(\frac{\delta c_p}{c_p}\right)^2 + \left(\frac{\delta \Delta T}{\Delta T}\right)^2\right]^{0.5} \quad (16)$$

6. Uncertainty in heat transfer coefficient

$$h_t = \frac{Q_u}{A_p \times (T_p - T_f)} = \frac{Q_u}{A_p \times \Delta T_f}$$

$$\frac{\delta h_t}{h_t} = \left[\left(\frac{\delta Q_u}{Q_u}\right)^2 + \left(\frac{\delta A_p}{A_p}\right)^2 + \left(\frac{\delta \Delta T_f}{\Delta T_f}\right)^2\right]^{0.5} \quad (17)$$

7. Uncertainty in Nusselt number

$$Nu_{rs} = \frac{h_t D_H}{K_a}$$

$$\frac{\delta Nu_{rs}}{Nu_{rs}} = \left[\left(\frac{\delta D_H}{D_H}\right)^2 + \left(\frac{\delta h_t}{h_t}\right)^2 + \left(\frac{\delta K_a}{K_a}\right)^2\right]^{0.5} \quad (18)$$

8. Uncertainty in Reynolds Number

$$Re = \frac{V.D_H}{\nu_a} = \frac{\rho_a V D_H}{\mu}$$

$$\frac{\delta Re}{Re} = \left[\left(\frac{\delta D_H}{D_H}\right)^2 + \left(\frac{\delta V}{V}\right)^2 + \left(\frac{\delta \rho_a}{\rho_a}\right)^2 + \left(\frac{\delta \mu}{\mu}\right)^2\right]^{0.5} \quad (19)$$

9. Uncertainty in friction factor

$$f_{rs} = \frac{2(\Delta_p)_d D_H}{4 \rho_a L_t V^2}$$

$$\frac{\delta f_{rs}}{f_{rs}} = \left[\left(\frac{\delta D_H}{D_H}\right)^2 + \left(\frac{\delta V}{V}\right)^2 + \left(\frac{\delta L_t}{L_t}\right)^2 + \left(\frac{\delta \rho_a}{\rho_a}\right)^2 + \left(\frac{\delta (\Delta_p)_d}{(\Delta_p)_d}\right)^2\right]^{0.5} \quad (20)$$

10. Uncertainty in thermo-hydraulic performance parameter

$$\eta_p = (Nu_{rs}/Nu_{ss})/(f_{rs}/f_{ss})^{0.33}$$

$$\frac{\delta \eta_p}{\eta_p} = \left[\left(\frac{\delta Nu_{rs}}{Nu_{rs}}\right)^2 + \left(\frac{\delta f_{rs}}{f_{rs}}\right)^2\right]^{0.5} \quad (21)$$

As the uncertainty calculation was done on a single test run (constant Reynolds number), the uncertainty analysis for complete test run for single geometry (complete set of Reynolds number) was carried out and results are presented in Table.2 for the experimental data.

Table 2 Range of uncertainty in the measurement of essential parameters

Sr. No.	Parameters	Error range, %
1.	Heat transfer coefficient (h_t)	3.98 – 6.12
2.	Nusselt number (Nu_{rs})	3.89 – 6.55
3.	Friction Factor (f_{rs})	2.24– 4.15
4.	Thermo-hydraulic performance parameter (η_p)	3.45 – 6.89

Results and discussion

The Nu_{rs} and f_{rs} descriptions of an impingement jet solar air passage roughened with multiple arcs protrusion ribs, calculated on the sources of investigational data collected for different stream and roughness factors, are discussed below.

Validation of experimental setup

The value of Nu_{ss} and f_{ss} calculated through experimental outcomes for a smooth channel have been compared with the outcomes obtained from the Dittus-Boelter equation [Eq.(22)] for the Nu_{ss}, and modified Blasius equation [Eq.(23)] for the f_{ss} Kumar et al., [1].
The Nu_{ss} for a smooth passage is given by the Dittus-Boelter equation as:

$$Nu_{ss} = 0.023Re^{0.8}Pr^{0.4} \quad (22)$$

The f_{ss} for a smooth passage is given by the modified Blasius equation as:

$$f_{ss} = 0.085Re^{-0.25} \quad (23)$$

The comparison of the experimental and estimated outcomes of Nu_{ss} and f_{ss} as a function of the Re is shown in Fig. 3 (A-B) respectively. The average absolute percentage deviation of the experimental Nu_{ss} is 5.78% from the value predicted by Eq. (22), and the average absolute percentage deviation of the present experimental f_{ss} is 4.98% from the value predicted by Eq.(23). Thus there is a good agreement between the predicted values and the experimental values of the Nu_{ss} and f_{ss}. This ensures the accuracy of the experimental data obtained from the present setup within reasonable limits.

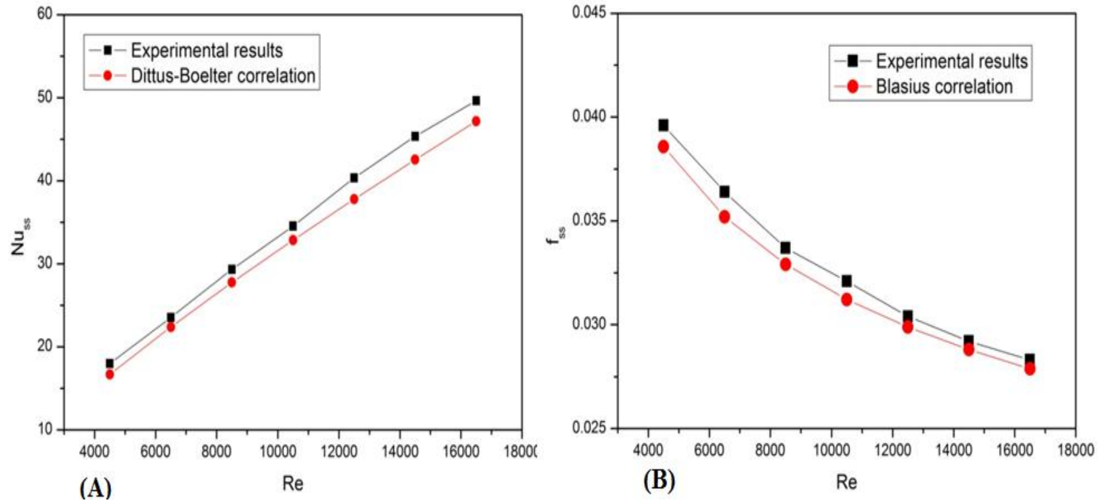

Fig.3 Comparison of experimental results with correlation results (A) Nu_{ss} (B) f_{ss}.

Heat and fluid flow

The experimental analysis has been perforated for a blockage solar air passage with sperical obtacles on a abosrber plate, and the results are discussed in this section. The results of D_S/D_H on Nu_{rs}, Nu_{rs}/Nu_{ss}, f_{rs} and f_{rs}/f_{ss} for air flow are represented in a SAP. The outcomes have been compared with those obtained in case of without obstacles surface working under similar experimental conditions.

The outcomes of Nu_{rs} have been presented as a function of Re for the various values of D_S/D_H in Fig.4 (A), and for constant values of the other blockage parameters such as Y_S/D_s= 0.152 and Y_S/D_s=0.152. It has been seen that the Nu_{rs} increase with increase in the D_S/D_H and attains a highest value matching to a D_S/D_H value of 0.195 in the range of the parameters studied. In all cases, the presence of a surface with spehrical blockage produces maximum Nu_{rs} compares to the without spehrical blokage passage. The spherical blockage can lead to superior Nu_{rs} performance because of the scondary flow vortices induced by the upper part of spherical blockage. These secondary flow vortices have the form of more than one counter rotating vortices, which carry cold air from the middle core region towards the spherical blockage surfaces. These secondary flow vortices interect with the primary stream, thus affecting the flow reattachment and recirculation between spherical blockage and interrupt the boundary layer enlargement down ward of the re-attachment regions.

Fig.4 (B) presents the values of Nu_{rs} as function of D_S/D_H for the selected Re values where a superior in the values corresponding to a D_S/D_H=0.195 for all Re. The outcomes of Nu_{rs}/Nu_{ss} have been presented as a function of Re for the various values of D_S/D_H in Fig.5 (A), and for constant values of the other blockage parameters such as Y_S/D_s= 0.152 and Y_S/D_s=0.152. It has been seen that the Nu_{rs}/Nu_{ss} increase with increase in the D_S/D_H and attains a highest value matching to a D_S/D_H value of 0.195 in the range of the parameters studied. Fig.5 (B) presents the values of Nu_{rs}/Nu_{ss} as function of D_S/D_H for the selected Re values where a superior in the values corresponding to a D_S/D_H=0.195 for all Re.

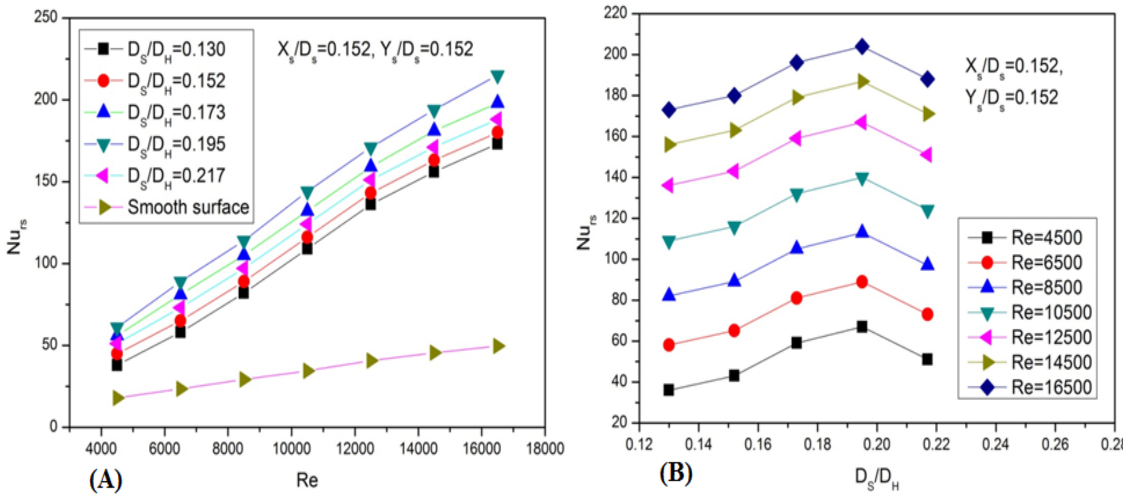

Fig.4 (A) Variation of Nu_{rs} with Re at different D_S/D_H (B) Variation of Nu_{rs} with D_S/D_H at selected Re.

The outcomes of f_{rs} have been represents as a function of Re for the various values of D_S/D_H in Fig.6 (A), and for constant values of the other blockage parameters such as Y_S/D_s= 0.152 and Y_S/D_s=0.152. It has been seen that the f_{rs} increase with increase in the D_S/D_H and attains a highest value matching to a D_S/D_H value of 0.217 in the range of the parameters studied. In all cases, the presence of a surface with spehrical blockage produces maximum f_{rs} compares to the without spehrical blokage passage.

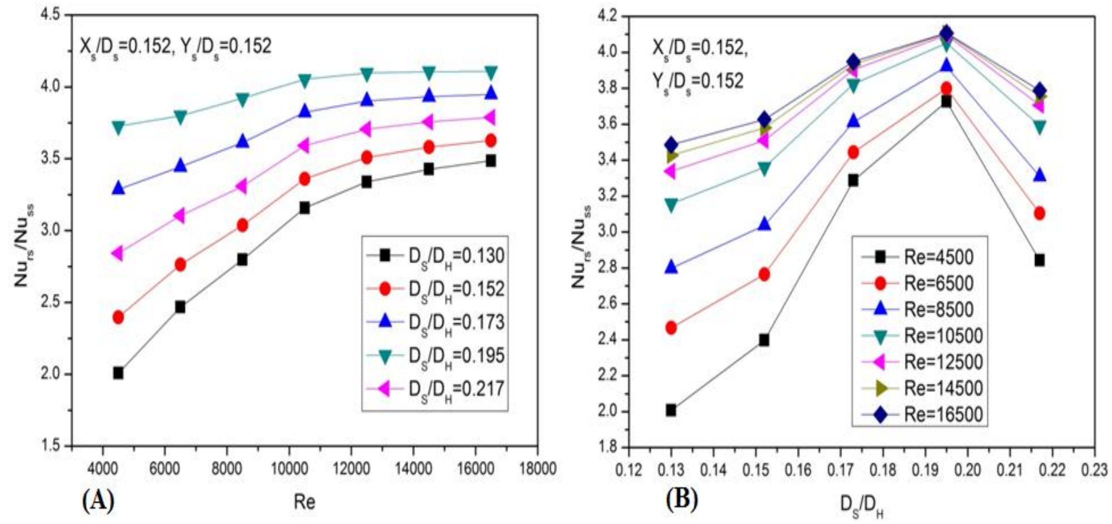

Fig.5 (A) Variation of Nu_{rs}/Nu_{ss} with Re at different D_S/D_H (B) Variation of Nu_{rs}/Nu_{ss} with D_S/D_H at selected Re.

Fig.6 (B) presents the values of f_{rs} as function of D_S/D_H for the selected Re values where a superior in the values corresponding to a D_S/D_H=0.217 for all Re. The outcomes of

f_{rs}/f_{ss} have been represents as a function of Re for the various values of D_S/D_H in Fig.7 (A), and for constant values of the other blockage parameters such as Y_S/D_s= 0.152 and Y_S/D_s=0.152. It has been seen that the f_{rs}/f_{ss} increase with increase in the D_S/D_H and attains a highest value matching to a D_S/D_H value of 0.217 in the range of the parameters studied. Fig.7(B) presents the values of f_{rs}/f_{ss} as function of D_S/D_H for the selected Re values where a superior in the values corresponding to a D_S/D_H=0.217 for all Re.

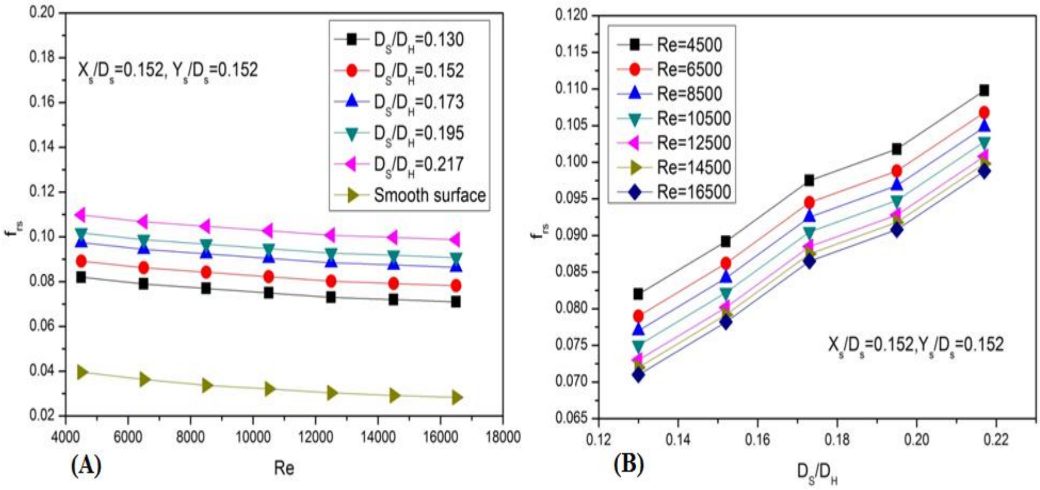

Fig.6 (A) Variation of f_{rs} with Re at different D_S/D_H (B) Variation of f_{rs} with D_S/D_H at selected Re.

Thermal hydraulic performance

The SAP with spherical blockage results in highest Nu_{rs}/Nu_{ss} as well as f_{rs}/f_{ss} as compared to without spherical blockage SAP. So a overall thermal performance needs to the calculated that takes into account both Nu_{rs}/Nu_{ss} as well as f_{rs}/f_{ss} to evaluate to usefulness. A overall thermal performance parameter based on equal pumping power explained by Webb and Eckert [18], Kumar and Kim [19] and Kumar et al. [20] considered both the Nu_{rs}/Nu_{ss} and f_{rs}/f_{ss} enhancement. The outcomes of η_p have been represents as a function of Re for the various values of D_S/D_H in Fig.8, and for constant values of the other blockage parameters such as Y_S/D_s= 0.152 and Y_S/D_s=0.152. It has been seen that the η_p increase with increase in the D_S/D_H and attains a highest value matching to a D_S/D_H value of 0.195 in the range of the parameters studied.

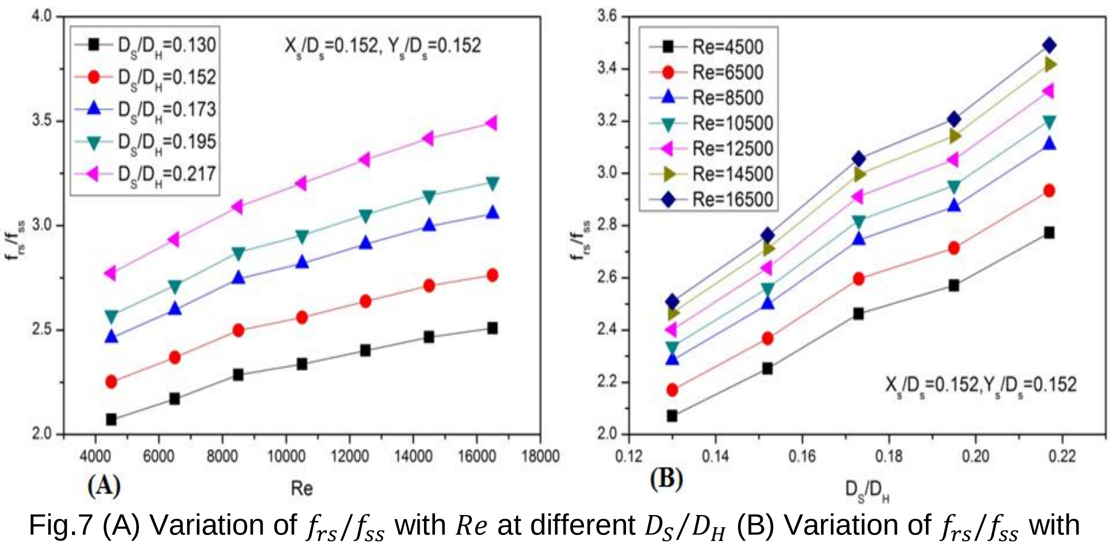

Fig.7 (A) Variation of f_{rs}/f_{ss} with Re at different D_S/D_H (B) Variation of f_{rs}/f_{ss} with D_S/D_H at selected Re.

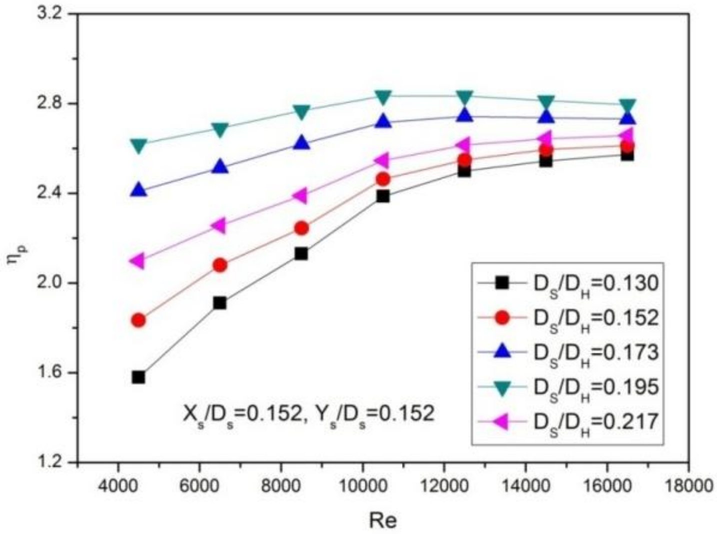

Fig.8 Variation of η_p with Re at different D_S/D_H.

Conclusions

A SAP roughened with sphere blockage was experimentally analysis for variation in sphere of
diameter. The following conclusions are drawn;

- Attached a sphere type blockage in the inner side of heated plate reults in considerable enhancement inn heat transfer of fluid flow SAP, the enhancement is a strong function of diameter of spherical blockage.
- An increase in heat transfer while decreases in pressure drop with increase in Reynolds number values is observed.
- The highest values of Nu_{rs} and Nu_{rs}/Nu_{ss} are observed for a spherical dimaeter blockage SAP with a D_S/D_H=0.195.
- The maximum values of f_{rs} and f_{rs}/f_{ss} are observed for a spherical dimaeter blockage SAP with a D_S/D_H=0.217.
- The superior value of overall thermal performance parameter is 2.83 corresponding to D_S/D_H of 0.195.

Nomenclature

A_p	Heated plate surface area, (m^2)
A_o	Orifice area, (m^2)
C_{do}	Coefficient of discharge
C_p	Specific heat of air, $(J/kg\ K)$
D_H	Hydraulic diameter of channel, (m)
D_S	Diameter of sphere, (m)
D_S/D_H	Relative sphere diameter
f_{rs}	Friction factor of roughened obstacle
f_{ss}	Friction factor without obstacle
h_t	Convective heat transfer coefficient,(W/m^2K)
H_P	Height of passage, (m)
K_a	Thermal Conductivity of air,(W/mK)
L_t	Length of test section, (m)
m_a	Mass flow rate of air, (kg/s)
Nu_{rs}	Nusselt number of obstacle surface
Nu_{ss}	Nusselt number of surface without obstacle
$(\Delta_p)_d$	Pressure drop across test section, (Pa)
$(\Delta_p)_o$	Pressure drop across orifice plate, (Pa)
Q_u	Useful energy gain, (W)

Re	Reynolds number of fluid
T_f	Average temperature of air, (K)
T_i	Inlet temperature of air, (K)
T_o	Outlet temperature of air, (K)
T_p	Plate temperature of air, (K)
U	Mean air velocity, (m/s)
V	Velocity of air, (m/s)
W_P/H_P	Passage aspect ratio
W_P	Width of passage, (m)
X_S	Stream wise spacing, (m)
X_S/D_S	Realtive stream wise spacing
Y_S	Span wise spacing, (m)
Y_S/D_S	Realtive span wise spacing

Greek symbols

β_O	Open area ratio, (%)
β_R	Ratio of orifice meter to pipe diameter, dimensionless
ρ_a	Air density, (kg/m^3)
ν_a	Kinematic viscosity of air, (m^2/s)
η_p	Thermal hydraulic performance

References

[1] Kumar A, Kim M.H., Mathematical simulation on thermal performance of packed bed solar energy storage system, *Trans. of the Korean Hydrogen and New Energy Society* 26 (2015), pp. 331-338.

[2] Kumar et al., Experimental study and correlation development for Nusselt number and friction factor for discretized boken V-pattern baffle solar air channel, *Experimental Thermal and Fluid Science*, 31 (2017), pp.56-75.

[3] Kumar, A, Kim M.H, Solar air-heating system with packed-bed energy-storage systems, *Renewable and Sustainable Energy Reviews*, 72 (2017), pp. 215–227.

[4] Kumar, A, Kim M.H, CFD analysis on thermal hydraulic performance of a SAH duct with multi V-shape roughened ribs, *Energies* 9 (6), 2016, pp.1-18.

[5] Zhou, G, Ye Q, Experimental investigations of thermal and flow characteristics of curved trapezoidal winglet type vortex generators, *Appl. Therm. Eng* 37 (2012), pp. 241-248.

[6] Park et al., Heat transfer in rectangular duct with perforated blockages and dimpled side walls. *International Journal of Heat and Mass Transfer* 97 (2016), pp.224-231.

[7] Sangtarash F, Shokuhmand H. Experimental and numerical investigation of the heat transfer augmentation and pressure drop in simple, dimpled and perforated dimpled louver fin banks with an in-line or staggered arrangement. *Applied Thermal Engineering* 82 (2015), pp.194-205.

[8] Bhushan B, Singh R. Nusselt number and friction factor correlations for solar air heater duct having artificially roughened absorber plate. *Solar Energy* 85 (2011), pp.1109-1118.

[9] Chang et al., Thermal performance comparison between radially rotating ribbed parallelogram channels with and without dimples. *International Journal of Heat and Mass Transfer* 55 (2012), pp.3541-3559.

[10] Shen et al.,Numerical predictions on fluid flow and heat transfer in U-shaped channel with the combination of ribs, dimples and protrusions under rotational effects. *International Journal of Heat and Mass Transfer* 80 (2015), pp.494-512.

[11] Kumar A, Kim M.H., Numerical study on overall thermal performance in SAH duct with compound roughness of V-shaped ribs and dimples. *Journal of the Korean Solar Energy Society* 35 (2015), pp.1-16.

[12] Lian et al., Heat transfer and friction factor correlations for solar air collectors with hemispherical protrusion artificial roughness on absorber plate. *Solar Energy* 118 (2015), pp.460-468.
[13] Negi D.S., Pattamatta A., Profile shape optimization in multi-jet impingement cooling of dimpled topologies for local heat transfer enhancement, *Heat Mass Transfer*, 36 (2014), pp. 145-158.
[14] Jin et al., Numerical investigation of heat transfer and fluid flow in a solar air heater duct with multi V-shaped ribs on the absorber plate, *Energy* 89 (2015), pp.178-190.
[15] Ekadewi et al., Numerical studies on the effect of delta-shaped obstacles' spacing on the heat transfer and pressure drop in v-corrugated channel of solar air heater, *Solar Energy* 131 (2016), pp.47–60.
[16] ASHRAE Standard 93, Method of testing to determine the thermal performance of solar collectors. Atlanta, GA: American Society of Heating, *Refrigeration and Air Conditioning Engineers* (2003).
[17] Kline S.J., Mcclintock F.A., Describing uncertainties in single sample experiments,*Mechanical Engineering* 75 (1953), pp.3-8.
[18] Webb R.L, Eckert E.R.G, Application of rough surface to heat exchanger design, *Int. J.*
Heat Mass Transfer 15 (1972), pp.1647–1658.
[19] Kumar A and Kim MH, Thermal hydraulic performance in a solar air heater channel with multi V-type perforated baffles, *Energies* 9 (7), 2016, pp.564.
[20] Kumar et al. Experimental investigations on thermo-hydraulic performance due to flow-attack-angle in multiple V-ribs with gap in a rectangular duct of solar air heaters, *Journal of sustainable Energy & environment* 4 (1), 2013, pp.1-7.